Eur. Phys. J. B **59**, 155–165 (2007)
DOI: 10.1140/epjb/e2007-00283-3

THE EUROPEAN PHYSICAL JOURNAL B

First-principles investigation of structural, electronic and optical properties of IVA group spinel nitrides

Hao Wang[1,a], Ying Chen[2], Yasunori Kaneta[2], and Shuichi Iwata[1]

[1] Department of Human and Engineering Environmental Studies, Graduate School of Frontier Science, The University of Tokyo, Kashiwanoha 5-1-5, Kashiwa, Chiba 277-8563, Japan
[2] Department of Quantum Engineering and Systems Sciences, School of Engineering, The University of Tokyo, Hongo 7-3-1 Bunkyo-ku, Tokyo 113-8656, Japan

Received 23 May 2007 / Received in final form 23 August 2007
Published online 17 October 2007 –

Abstract. The Si_3N_4 and Ge_3N_4 are important structural ceramics with many applications because of their attractive high temperature and oxidation resistant properties. The high-pressure and high-temperature spinel phases of these two materials were noticed to have wide, direct electronic band gaps. Other single and double spinel nitrides formed from IVA and IVB group elements have also attracted much attention. Present research focuses on selecting a special substance with promising optical properties and stability besides the attractive electronic properties. The formation energies of spinel nitrides are calculated and stabilities of a group of spinel nitrides are discussed, the structural and electronic properties of them are investigated in detail. By random phase approximation (RPA), the optical properties of spinel nitrides are researched. We obtain that γ-$SiGe_2N_4$ has some promising properties with potential technological applications from various aspects. The band transitions which contribute most to the peak of ε_2 have been identified. An assumption is proposed to raise the peak of ε_2.

PACS. 71.20.Nr Semiconductor compounds – 71.15.Mb Density functional theory, local density approximation, gradient and other corrections

1 Introduction

The polymorph formed from elements in group-IV and group-V is an interesting and important class of materials. Silicon nitride (Si_3N_4) is a well-known material because of its high fracture toughness, hardness and wear resistance [1,2]. Another well-researched polymorph is Ge_3N_4. The existence of several solid phases and the phase transitions among them have been attracted for years. α (P31c, hp28), β (P6$_3$/m, hp14) and γ (spinel, Fd$\bar{3}$m, cF56) phases of Si_3N_4 and Ge_3N_4 are well-known by experiments [3–7]. The forth phase, olivine phase, has also been reported and investigated by ab initio calculation [8]. The crystal structure of α phase is trigonal and that of β phase is hexagonal. Both α and β phases for Si_3N_4 and Ge_3N_4 are stable under an ambient pressure, while the β phase is more stable than α phase. The α phase transits into the β phase upon heating, however the $\beta \rightarrow \alpha$ phase transition has not yet been observed. The high pressure phases of them are the γ phase. The γ-Si_3N_4 was first synthesized under a pressure of 15 GPa and at a high temperature of 2000 K [7]. The $\beta \rightarrow \gamma$ phase transition of Ge_3N_4 occurs near 12–15 GPa and above 1273 K [9]. β-Si_3N_4 transits to the γ phase by a fast reconstructive process at pressure above 20 GPa [10]. It has been shown that the γ-Si_3N_4 and γ-Ge_3N_4 have wide, direct electronic band gaps that are comparable to those of the developed solid state promising optoelectronic materials such as GaN, InN, AlN [11]. γ-C_3N_4 is a super hard substance predicted theoretically by Teter et al. and its bulk modulus is even larger than the value of diamond [12]. γ-Sn_3N_4 was synthesized both by a rapid solid metathesim reaction [13] and from an annealed tin amidimide precursor at ambient pressure [14]. Bulk γ-Sn_3N_4 was prepared by pyrolysis of a tin amide imide precursor, $Sn(NH_2)_2NH$ [15,16]. Thin films containing γ-Sn_3N_4 was deposited using several variations of reactive sputtering and atmospheric chemical vapor deposition [17–21].

Encouraged by the results above, the stabilities of the spinel nitrides of IVA and IVB group have been investigated with the orthogonalized linear combination of atomic orbitals (OLCAO) method [22–25]. In present paper, we focus on the stabilities and optical properties of those materials to seek a new optical material. At first according to our purpose, the appropriate semiconductors are selected based on the calculation results by OLCAO and relevant experiments, the stabilities of them are discussed further with full potential linearized augmented

[a] e-mail: oukou@gakushikai.jp

plane wave. The structural and electronic properties of them are investigated in detail. Then by random phase approximation (RPA), the optical properties of spinel nitrides are obtained and discussed.

The calculation method and parameters are described in the next section, followed by results and discussions in Section 3. Conclusions are given in Section 4.

2 Calculation method and parameters

In order to investigate the structural and electronic properties of the spinel nitrides, we perform calculations based on the density functional theory (DFT) and local density approximation (LDA) with generalized gradient approximation (GGA) [26,27]. The FLAPW method using a scalar relativistic effect embodied in the WIEN2k code is employed [28]. The linearized augmented plane waves (LAPW) and augmented plane wave with local orbitals (APW+lo) are applied as basis. The "physically important" l-quantum numbers are treated by APW+lo but the higher l by LAPW [29]. Local orbital(LO) is used for low-lying valence states: semi-core states. Electronic configurations for relevant elements are listed as following:

C: $(2s^2)$ $2p^2$,
Si: $(2p^6)$ $3s^2$ $3p^2$,
Ge: $(3d^{10})$ $4s^2$ $4p^2$,
Sn: $(4p^6$ $4d^{10})$ $5s^2$ $5p^2$,
N: $(2s^2)$ $2p^3$.

The configurations in parenthesis are treated for semi-core states. The PBE-GGA is employed for the exchange and correlation potential [27]. For the potential and charge density representation, the maximum l value for partial waves used inside atomic spheres is 10 and the one used in the computation of non-muffin-tin matrix elements is 4. In the interstitial region they are represented by Fourier series and the plane wave cut-offs of calculations are all above 25 Ry. The tetrahedron method is used for efficient sampling of the first Brillouin zone (BZ) [30]. 47 k-points are used in the irreducible BZ, which correspond to 1000 k-points in the whole BZ. For the internal structural parameters, a reverse-communication trust-region quasi-Newton method from the Port library [31] is employed to determine the equilibrium position of all individual atoms. The optimization is performed with the constraint of maintaining the corresponding space-group symmetry.

Spinel compounds belong to the space group $Fd\bar{3}m$. The spinel structure is geometrically a ternary structure with stoichiometry AB_2X_4, where A and B are respectively tetrahedrally coordinated and octahedrally coordinated cations and X are anions. The spinel structure is shown in Figure 1. The yellow balls are the tetrahedrally coordinated cations A to the blue X anions, the green ones are the octahedrally coordinated cations B to the blue X anions. The ideal atomic positions of spinel phase materials are shown in Table 1.

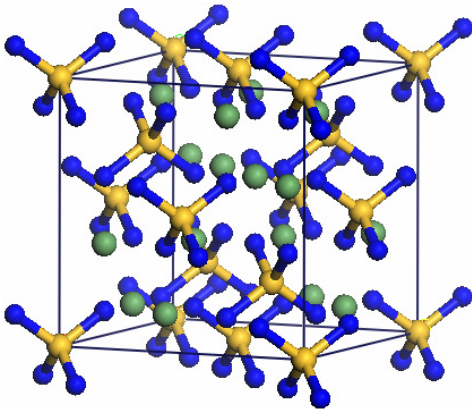

Fig. 1. (Color online) Crystal-structure of γ-AB_2X_4. The yellow balls are the tetrahedral cations A to the blue X anions, the green ones are the octahedral cations B to the blue X anions.

Table 1. Wyckoff parameters for each atomic species of the spinel structure.

Atom	Wyckoff	Coordinates
A	8a	$(\frac{1}{8},\frac{1}{8},\frac{1}{8})$, $(\frac{7}{8},\frac{3}{8},\frac{3}{8})$
B	16d	$(\frac{1}{2},\frac{1}{2},\frac{1}{2})$, $(\frac{1}{4},\frac{3}{4},0)$, $(\frac{3}{4},0,\frac{1}{4})$, $(0,\frac{1}{4},\frac{3}{4})$
N	32e	(x,x,x),$(\bar{x}+\frac{3}{4},\bar{x}+\frac{1}{4},x+\frac{1}{2})$, $(\bar{x}+\frac{1}{4},x+\frac{1}{2},\bar{x}+\frac{3}{4})$, $(x+\frac{1}{2},\bar{x}+\frac{3}{4},\bar{x}+\frac{1}{4})$, $(x+\frac{3}{4},x+\frac{1}{4},\bar{x}+\frac{1}{2})$, $(\bar{x},\bar{x},\bar{x})$, $(x+\frac{1}{4},\bar{x}+\frac{1}{2},x+\frac{3}{4})$, $(\bar{x}+\frac{1}{2},x+\frac{3}{4},x+\frac{1}{4})$

3 Results and discussions

The spinel nitrides of IVA and IVB group have been investigated with the orthogonalized linear combination of atomic orbitals (OLCAO) method [22–25]. In those works, thirty-nine single and double spinel nitrides have been explored from total forty-nine combinations of group IVA element carbon, silicon, germanium and group IVB element titanium, zirconium and hafnium in which only γ-Hf_3N_4, γ-$ZrHf_2N_4$, γ-$HfZr_2N_4$ are included among those combinations containing hafnium.

According to the works, the formation energy of the double nitride can be estimated with respect to the single nitrides as following:

$$\Delta E_t = E_t(AB_2N_4) - \left[\frac{1}{3}E_t(A_3N_4) + \frac{2}{3}E_t(B_3N_4)\right]. \quad (1)$$

This formation energy gives information on the stability of a double spinel compound when it is synthesized from two terminal single spinel nitrides. The value of ΔE_t at the equilibrium geometry corresponds to the free energy of the compound at zero temperature and zero pressure. In fact, the discussion of such a kind of formation with a temperature effect should consider the free energy instead

Table 2. List of spinel nitrides γ-AB_2N_4 in this study.

A \ B	C	Si	Ge	Sn
C		γ-CSi_2N_4	γ-CGe_2N_4	
Si		γ-Si_3N_4	γ-$SiGe_2N_4$	
Ge		γ-$GeSi_2N_4$	γ-Ge_3N_4	
Sn			γ-$SnGe_2N_4$	γ-Sn_3N_4

of internal energy at the ground state. However, the internal energy still gives important information about the stability.

With the purpose of finding new spinel materials with satisfied stability and attractive optical property, we at first select several substances as the initial target substances. It is reasonable to take the synthesized γ-Si_3N_4, γ-Ge_3N_4 and γ-Sn_3N_4 and double spinel nitrides constituted from element Si, Ge and Sn as candidates. γ-C_3N_4 and the double spinel nitrides containing element C are also included. In addition, we further skip those spinel nitrides of IV groups with poor stability, and only pay attention to ones having negative value or slightly positive values of formation energy based on previous calculations [22–25]. As a result, totally eight single and double spinel nitrides are selected in present calculation: γ-Si_3N_4, γ-Ge_3N_4, γ-Sn_3N_4, γ-CGe_2N_4, γ-CSi_2N_4, γ-$GeSi_2N_4$, γ-$SiGe_2N_4$ and γ-$SnGe_2N_4$, which are listed in Table 2.

3.1 Structural stability

Total energy calculations are performed by using FLAPW approach. With total energies E_t, the formation ΔE_t can be calculated. In order to obtain the intrinsic ground state property, we calculate the formation energy with respect to the segregation limit which is defined as the concentration average of the internal energies at the ground state of elemental substances. For a compound $A_xB_yC_z$, the formation energy ΔE_t can be expressed generally as following equation:

$$\Delta E_t = E_t(A_xB_yC_z) - \left[\frac{x}{x+y+z}E_t(A) + \frac{y}{x+y+z}E_t(B) + \frac{z}{x+y+z}E_t(C)\right]. \quad (2)$$

In present session, apart from the spinel materials, the graphite for C whose diamond phase is also stable but should be synthesized by cooling from high temperature with simultaneous expansion from high pressure [32], diamond structure for Si, Ge and Sn are calculated as the references. For N element, the authors employ the diatomic gas N_2 as the elemental substance. The formation energies of spinel nitrides by equations (1) and (2) are calculated and shown in Table 3. The formation energies by OLCAO from other works are also listed.

γ-Si_3N_4 was formed in experiment in which silicon single crystals were placed in a nitrogen pressure medium served also as a reactant [7]. Our results show a large negative formation energy of –0.93 eV/atom. Both our calculation and experimental results verify that γ-Si_3N_4 can be metastable in appropriate situation since α- and β-Si_3N_4 are more stable [8].

For γ-Ge_3N_4, our calculation exhibits a positive formation energy of 0.398 eV/atom. Serghiou et al. have shown that γ-Ge_3N_4 can be recovered to ambient conditions after reaction of germanium with nitrogen at pressures at least as low as 14 GPa [9], in which elemental germanium and molecular nitrogen were used. The difference between our result and the experiment can be attributed to the distinction between ground state in our calculation and actual experimental situation.

According to our calculation, γ-Sn_3N_4 is not a stable phase, whereas crystalline γ-Sn_3N_4 was successfully synthesized in both bulk and thin film forms by several groups. In the experiments, however, γ-Sn_3N_4 was not synthesized by elemental tin in a nitrogen pressure medium while segregation limit of our results are obtained with the total energies of diamond tin and molecular nitrogen. This difference can be the reason that in our calculation γ-Sn_3N_4 is unstable while it has actually been synthesized in experiment.

It is obtained by our calculation that the formation energies of γ-Si_3N_4, γ-CSi_2N_4, γ-$SiGe_2N_4$ and γ-$GeSi_2N_4$ are negative. γ-CSi_2N_4 and γ-$SiGe_2N_4$ are consistent with results of Ching et al. by OLCAO method. γ-$GeSi_2N_4$ is negative for formation energy in our result while is positive in results of Ching et al. Dong predicted by alloy formation energy that γ-$GeSi_2N_4$ is a stable phase [36]. According to the results of Ching et al., formation energy of γ-CGe_2N_4 and γ-$SnGe_2N_4$ are zero and positive respectively [25]. However in our calculation, both are negative by equation (1) but positive by equation (2). The difference between these can be attributed to different definitions of formation energy and theoretical methods in calculations. From the results of our calculations about relative stability (Eq. (1)) and intrinsic stability (Eq. (2)), it can be obtained that γ-$SiGe_2N_4$ could be synthesized not only by γ-Si_3N_4 and γ-Ge_3N_4 but also by elemental substances. γ-CSi_2N_4 and γ-$GeSi_2N_4$ could be synthesized in experiment. Whereas it is possible for γ-CGe_2N_4 and γ-$SnGe_2N_4$ to be synthesized in experiment.

For bulk modulus, γ-$GeSi_2N_4$ has a larger B of 264.8 GPa than 216.3 GPa in γ-Ge_3N_4. The same tendency γ-CSi_2N_4 and γ-CGe_2N_4, γ-Si_3N_4 and γ-$SiGe_2N_4$, γ-Sn_3N_4 and γ-$SnGe_2N_4$ have respectively. Although the bulk moduli decrease superficially as the valence electron number of these elements increases, it can not be obtained, however, that the elements in octahedrally coordinated sites play a critical rule on the bulk modulus. This is because the elements in tetrahedrally coordinated sites also have the same trend. For instance, γ-CSi_2N_4, γ-Si_3N_4 and γ-$GeSi_2N_4$, whose atomic number of the elements in tetrahedrally coordinated sites increase, have decreasing bulk moduli. The group of γ-CGe_2N_4, γ-$SiGe_2N_4$, γ-Ge_3N_4 and γ-$SnGe_2N_4$ has the same case.

Table 3. Summary of calculated properties of spinel nitrides.

Crystal	a(a.u.)	x	E_g(eV)	B(GPa)	B'	Formation energy (eV/atom)	
						by equation (2)	by equation (1)
γ-Si_3N_4	14.7526	0.3838	3.21	292.3	4.35	–0.93	
Experiment	14.7399[a]	0.3875[a]		317 ± 11[b]	2.3 ± 2.1[b]		
	14.6340[c]	0.3833[d]					
	14.6149[d]						
Other calculations	14.8102[e]	0.3843[f]	3.45[e]	280.1[e]	3.76[e]		
	14.8092[f]	0.3844[e]	3.45[f]	280[f]	3.48[f]		
γ-Ge_3N_4	15.7137	0.3833	1.90	216.3	4.61	0.39	
Experiment	15.6847[g]	0.3827[h]		296[h]	4.0[h]		
	15.5209[h]						
Other calculations	15.5165[e]	0.3830[i]	2.22[e]	268.6[e]	3.14[e]		
	15.4345[i]	0.3841[e]	2.17[i]	240[i]	4.5[i]		
γ-Sn_3N_4	17.2901	0.3839	0.19	156.4	4.7	0.93	
Experiment	17.0775[j]	0.3845[j]					
Other calculations	16.9214[k]	0.3839[k]	1.40[k]	187.2[k]	4.34[k]		
	16.9319[l]	0.3844[l]		186[l]	4.53[l]		
	16.9416[m]	0.3845[m]	1.29[m]	203.6[m]	4.98[m]		
γ-CSi_2N_4	13.9922	0.3743	1.44	329.7	4.26	–0.11	–0.05
Other calculations	14.2124[m]	0.3811[m]	1.34[m]	309.5[m]	2.72[m]		–0.09[m]
γ-CGe_2N_4	14.6982	0.3692	0.93	259.2	4.84	0.75	–0.07
Other calculations	14.6319[m]	0.37[m]	1.356[m]	266.0[m]	3.53[m]		0[m]
γ-$SiGe_2N_4$	15.3863	0.3785	1.58	241.7	4.48	–0.20	–0.16
Other calculations	15.2828[m]	0.3772[m]	1.85[m]	277.1[m]	3.02[m]		–0.04[m]
γ-$GeSi_2N_4$	15.0425	0.3868	3.04(id)	264.8	4.38	–0.66	–0.17
Other calculations	15.1193[m]	0.3900[m]	2.635[m]	258.3[e]	2.04[e]		0.06[m]
	14.8256[n]		3.3[n]	283[n]	3.93[n]		
γ-$SnGe_2N_4$	16.2319	0.3880	1.34(id)	192.2	5.13	0.33	–0.25
Other calculations	15.9899[m]	0.3895[m]	2.31[m]				0.01[m]

id means indirect band gap. [a]Reference [4]. [b]Reference [30]. [c]Reference [27]. [d]Reference [33]. [e]Reference [23]. [f]Reference [22]. [g]Reference [6]. [h]Reference [5]. [i]Reference [11]. [j]Reference [13]. [k]Reference [34]. [l]Reference [35]. [m]Reference [25]. [n]Reference [36].

3.2 Electronic band structure

The calculated band structures of γ-CGe_2N_4 and γ-$SnGe_2N_4$ are provided in Figure 2, which have not been presented previously to our knowledge. The band structures of other materials are provided in other papers [8,22–25]. The black arrows in γ-$SiGe_2N_4$ and γ-$GeSi_2N_4$ are the band transitions with the largest contribution to the peak of ε_2, which will be discussed later. Fermi energy is set to zero point of the energy in these graphs. The calculated band gaps are provided in Table 3.

For these substances, the bands appear typically to be semiconductors with a direct band gap at the Γ point except γ-$GeSi_2N_4$ and γ-$SnGe_2N_4$ which have an indirect band gap. Three parts of all band structures are clearly observed except that the upper valence band part of spinel nitrides containing carbon are wider enough to nearly touch the lower valence band part.

Our calculated band gaps of γ-Si_3N_4 and γ-Ge_3N_4 are 3.21 eV and 1.90 eV respectively. Comparing with other reports, one can see that the trends coincide, but the present calculations underestimate energy gaps by 7% to 14%. It is noticed that the our calculated energy gaps for γ-Sn_3N_4 and γ-$SnGe_2N_4$ are much narrower than the results of other calculations. Band gaps of γ-CGe_2N_4 and γ-$SiGe_2N_4$ are narrower whereas γ-CSi_2N_4 and γ-$GeSi_2N_4$ are wider than other calculations. Considering that the present calculation employs FLAPW [37], while others adopted OLCAO or ultrasoft pseudopotential, we expect these difference in values of band gap might be owing to the different theoretical treatments on exchange-correlation potential and basis function set used in expanding the wave functions. Since it is well-known that LDA calculations generally underestimate the band gap of semiconductors and insulators, the real band gaps of them must be wider.

According to our analysis, the top of valence band of all materials are mainly dominated by p-orbitals of N atoms. Cations in both tetrahedrally coordinated sites and octahedrally coordinated sites have almost equal contributions. However near the top of valence band, p-orbitals of Si atoms in octahedrally coordinated sites take more important parts in γ-Si_3N_4, γ-CSi_2N_4 and γ-$GeSi_2N_4$ while d-orbitals of Ge and Sn atoms in octahedrally coordinated sites are responsible in other five materials. Therefore, the

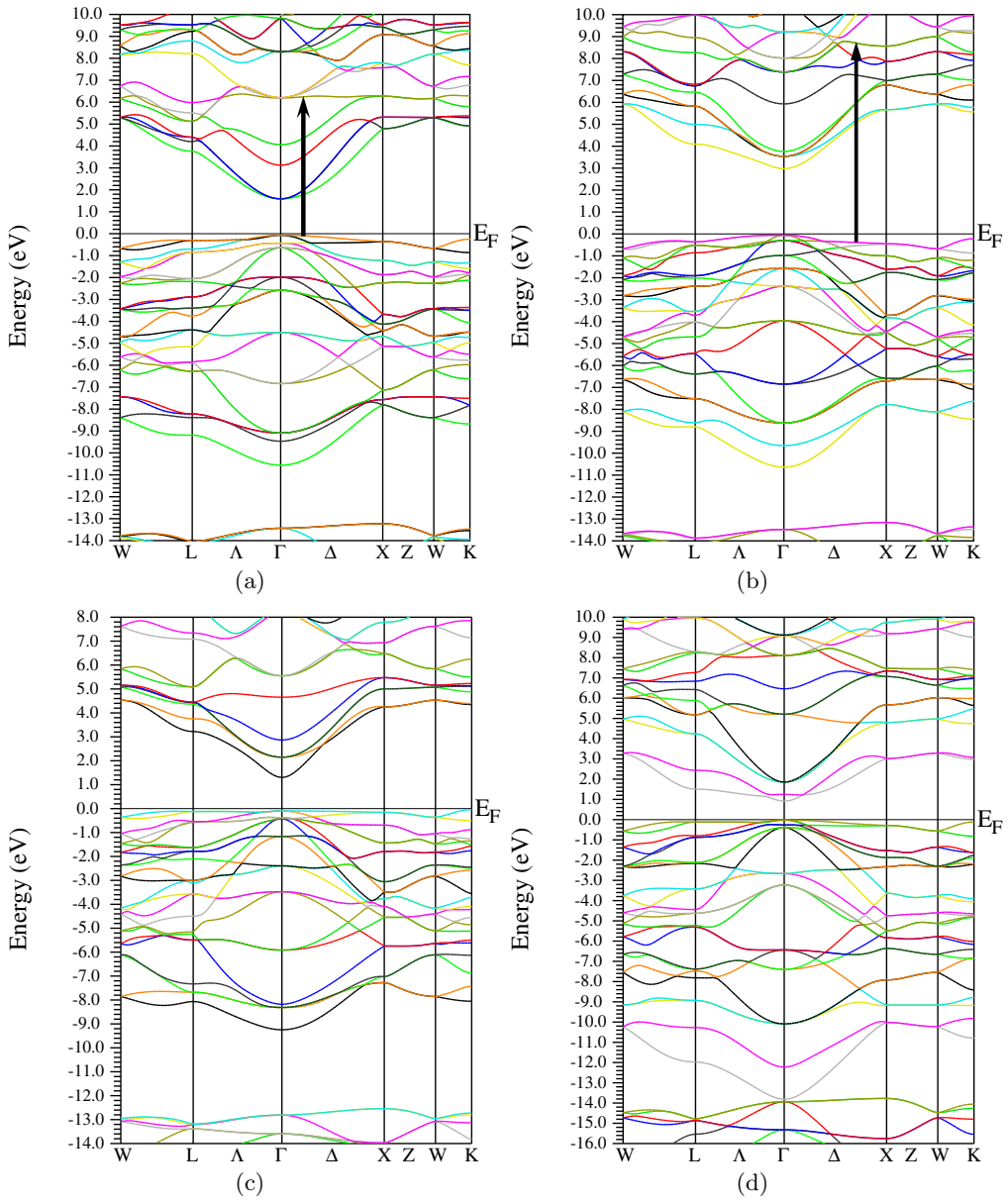

Fig. 2. Band structures of four materials. (a) γ-$SiGe_2N_4$, (b) γ-$GeSi_2N_4$, (c) γ-$SnGe_2N_4$, (d) γ-CGe_2N_4. The black arrows are the band transitions corresponding to the largest contribution to the peak of ε_2.

band gaps of spinel nitrides are reasonably affected by the cations in octahedrally coordinated sites.

Further investigation provides the trend of band gaps varying with respect to the valence electron number of elements which is shown in Figure 3. For single spinel nitrides, which are γ-Si_3N_4, γ-Ge_3N_4 and γ-Sn_3N_4, the band gap narrows as the valence number of IVA elements increases. This is also the case for the double spinel nitrides: the band gap of 1.44 eV in γ-CSi_2N_4 is wider than the one of 0.93 eV in γ-CGe_2N_4. γ-$SnGe_2N_4$ has a wider band gap of 1.34 eV than 0.19 eV of γ-Sn_3N_4. γ-Si_3N_4 and γ-$SiGe_2N_4$, γ-$GeSi_2N_4$ and γ-Ge_3N_4 have the same tendency respectively. It can be obtained that the band gap narrows as valence electron number of octahedrally coordinated cations increases.

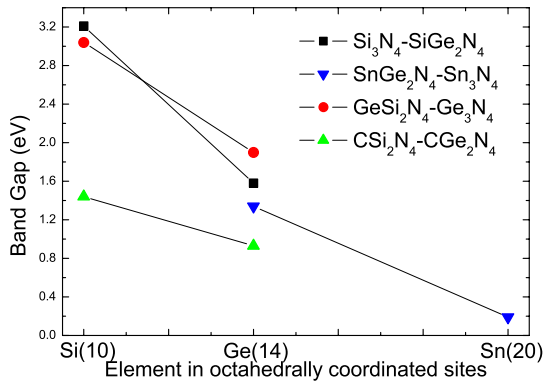

Fig. 3. Relation between band gap and valence electron number of element in octahedrally coordinated site. The number in parenthesis behind element is the valence electron number.

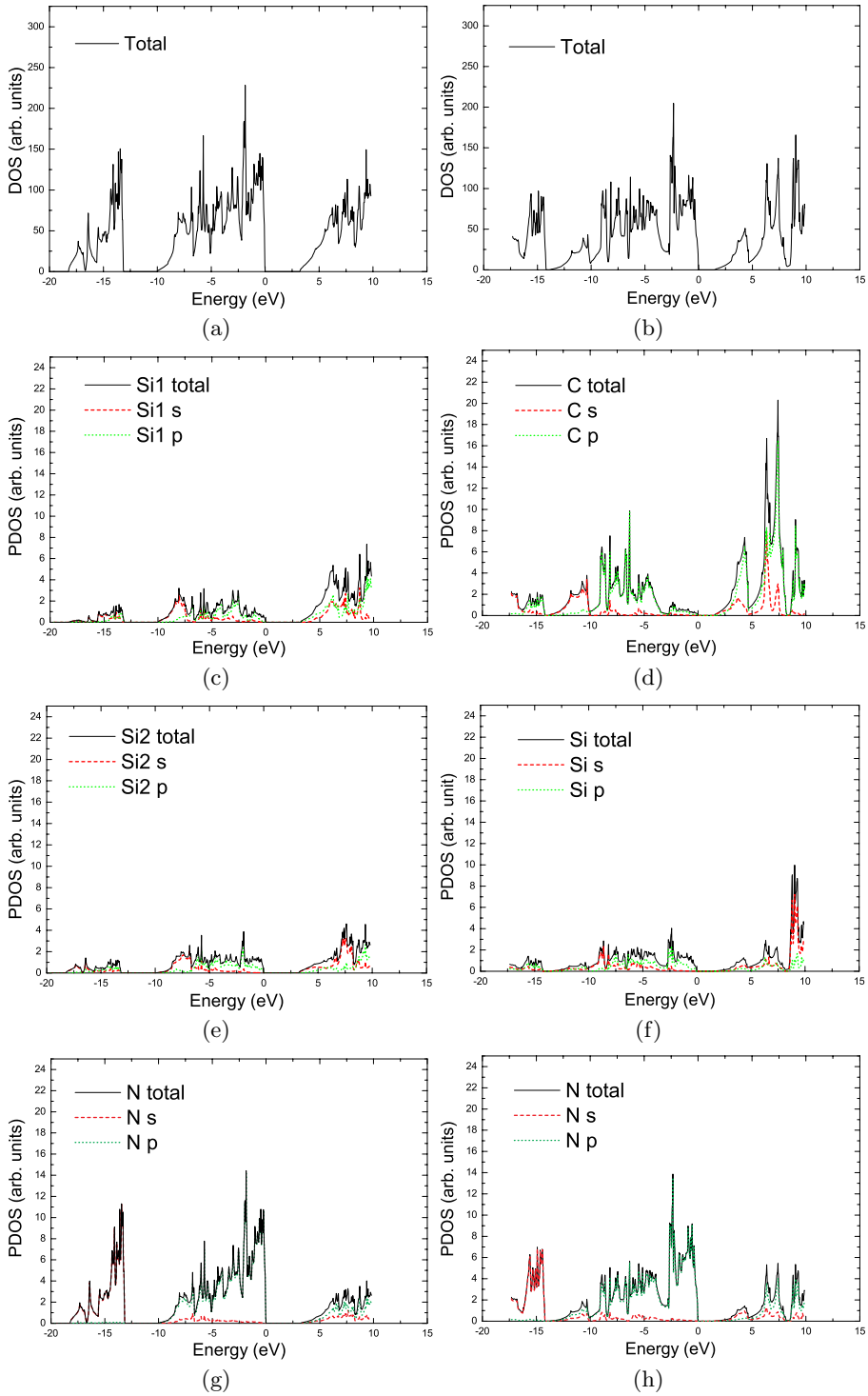

Fig. 4. (Color online) Total electronic density of states (a) γ-Si_3N_4, (b) γ-CSi_2N_4 and site-projected partial electronic density of states at the tetrahedrally coordinated sites Si1 (C), the octahedrally coordinated sites Si2 (Si), N sites. Fermi energy is at zero point.

This gives valuable information on how to enlarge the band gap in spinel nitrides of IVA group. However, this rule can not be applied to the C_3N_4 (not presented here), which has a band gap of 1.14 eV [22].

3.3 Density of states

The total electronic density of states (DOS) and site-decomposited partial density of states (PDOS) of γ-Si_3N_4, γ-CSi_2N_4, γ-$SnGe_2N_4$ and γ-CGe_2N_4 are shown in Figure 4.

The similarity of DOS and PDOS in γ-Si_3N_4 and γ-Ge_3N_4 (not shown here) is apparently attributed to the same structure and IVA group. The upper valence band part of γ-Si_3N_4, near the Fermi energy, is occupied by the Si atoms especially *p*-orbitals of those in both

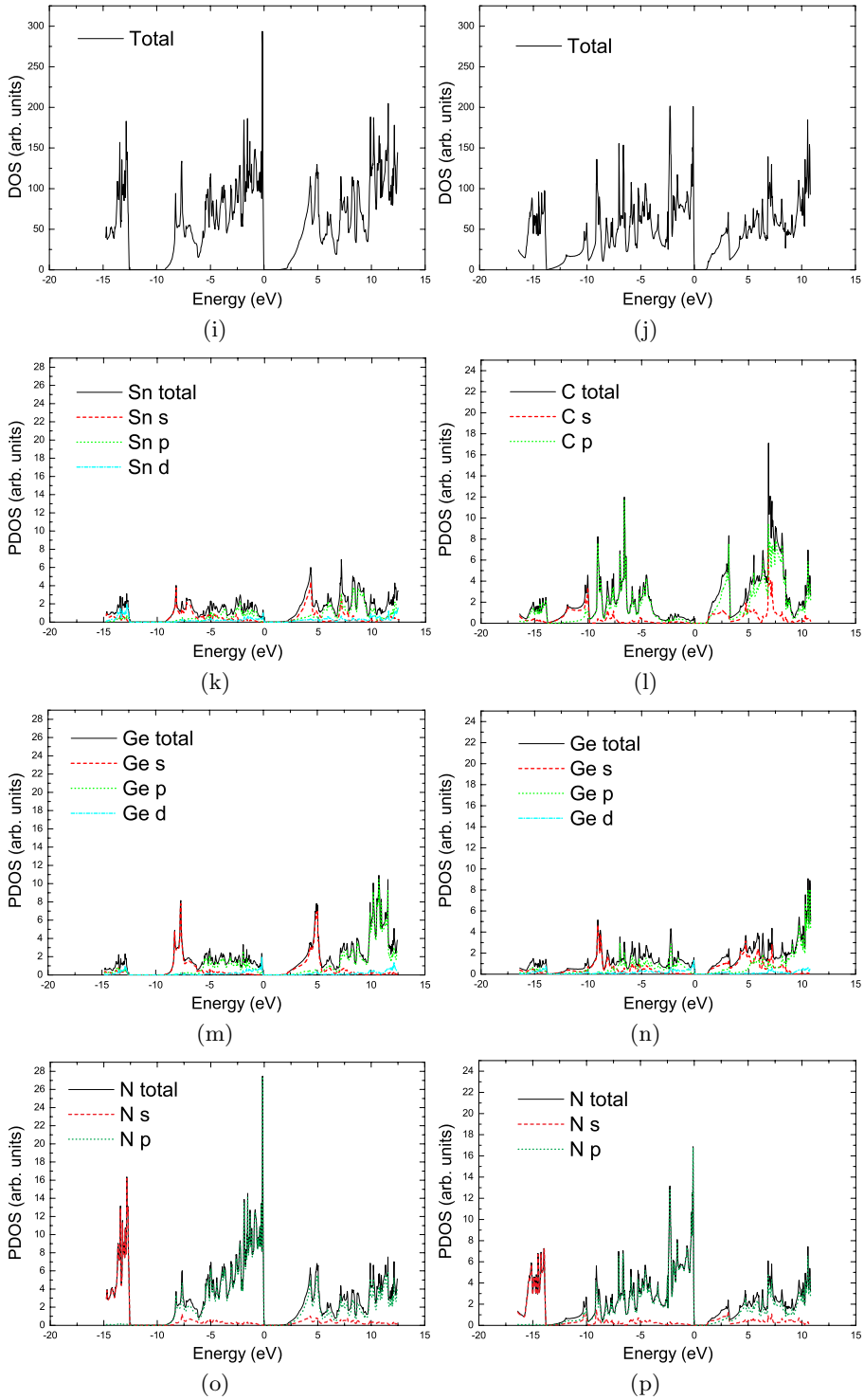

Fig. 4. *Continued* (Color online) Total electronic density of states (i) γ-$SnGe_2N_4$ and (j) γ-CGe_2N_4 and site-projected partial electronic density of states at the Sn (C), Ge, N sites. Fermi energy is at zero point.

tetrahedrally and octahedrally coordinated sites excluding N atoms.

In γ-$SnGe_2N_4$, the component of valence band is similar to that of γ-Si_3N_4 except that near the Fermi energy the *d*-orbitals of Ge in octahedrally coordinated atoms have more contributions to PDOS. This is also the case for γ-CGe_2N_4 and γ-Sn_3N_4 (not presented here). Unlike γ-Ge_3N_4, the *d*-orbitals of Ge and Sn besides N atoms, especially the ones in octahedrally coordinated sites, of these two materials possess the part near the Fermi energy.

In γ-CSi_2N_4 and γ-CGe_2N_4, the tetrahedrally coordinated C atoms contribute larger to the upper valence band than other elements in these sites of other substances. This is the reason that the spinel nitrides containing C have a large bulk modulus.

Table 4. Summary of optical properties of spinel nitrides.

Crystal	Photon energy (eV)	Peak value of ε_2	Static dielectric constants $\varepsilon_1(0)$	ω_p
γ-Si_3N_4	9.73	11.1	5.39	6.28
γ-Ge_3N_4	7.03→7.06	10.9	7.08	3.84
γ-Sn_3N_4	5.86	11.6	10	3.15
γ-CSi_2N_4	11.31→11.42	10.6	5.83	8
γ-CGe_2N_4	8.67 & 9.43	9.92	7.97	5.01
γ-$SiGe_2N_4$	6.65	13.1	6.46	4.46
γ-$GeSi_2N_4$	9.18→9.23	11.2	5.83	5.45
γ-$SnGe_2N_4$	6.65→6.76	10.1	7.62	3.07

3.4 Optical property

The Random Phase Approximation (RPA) is used to calculate ε, by which other optical properties, such as energy loss function, can be obtained [38].

According to Kramers-Kröing relation [39,40], through the imaginary part of the interband contribution to the dielectric tensor component ε_2,

$$\varepsilon_{i,j}^{\text{inter}}(\omega) = \frac{\hbar^2 e^2}{\pi m^2 \omega^2} \sum_{n,n'} \int_{\mathbf{k}} p_{i;n',n,\mathbf{k}} p_{j;n',n,\mathbf{k}} (f(\varepsilon_{n,\mathrm{k}}) - f(\varepsilon_{n',\mathrm{k}})) \delta(\varepsilon_{n',\mathbf{k}} - \varepsilon_{n,\mathbf{k}} - \omega) \quad (3)$$

the corresponding real part is obtained by

$$\varepsilon_1(\omega) = 1 + \frac{2}{\pi} \wp \int_0^\infty \frac{\omega' \varepsilon_2(\omega')}{\omega'^2 - \omega^2} d\omega' \quad (4)$$

where $\wp$ is integration principle value

$$\wp \int_0^\infty \equiv \lim_{\Delta \to 0} \left(\int_0^{\omega - \Delta} + \int_{\omega + \Delta}^\infty \right). \quad (5)$$

The frequency-dependent real and imaginary parts of the dielectric function for photon energies up to 34 eV are estimated. The results of the spinel nitrides are shown in Figure 5. The solid, dashed and dotted line represents $\varepsilon_1(\omega)$, $\varepsilon_2(\omega)$ and the energy loss function respectively. Because of the isotropy of the spinel structure, one of three directions of dielectric function is shown.

The imaginary dielectric function $\varepsilon_2(\omega)$ represents the optical absorption in these materials. It can be obtained that the optical conductivity becomes more effective as the peak of ε_2 increases, which means that a material becomes more conductive due to the absorption of electromagnetic radiation such as visible light, ultraviolet light, or γ radiation. Peak value of $\varepsilon_2(\omega)$ and its corresponding photon energy are shown in Table 4. Static dielectric constants, which is $\varepsilon_1(0)$ (excluding any contribution from lattice vibrations), and plasma frequency ω_p, which is the main peak in energy loss function, are also provided.

From the Table 4, γ-CSi_2N_4 and γ-$SnGe_2N_4$ have a plane absorption peak, whereas γ-CGe_2N_4 has two peaks of ε_2. we can obtain that γ-$SiGe_2N_4$ has the highest peak of ε_2 with a larger static dielectric constant of 6.46. Also the corresponding incident photon energy of peak of ε_2 is the second lowest one in all spinel nitrides. Comparing to the results by Ching et al. [23,34], our photon energies of γ-Si_3N_4, γ-Ge_3N_4, γ-Sn_3N_4, γ-$SiGe_2N_4$ and γ-$GeSi_2N_4$ are lower while the highest peaks are higher than theirs. The static dielectric constants of our results are also higher than theirs except for γ-$GeSi_2N_4$. Both calculations employ the RPA method, so the difference between the results should be attributed to the utilized basis, which results in difference in band structures.

However, γ-$SiGe_2N_4$ has low $\varepsilon_1(0)$ and peak of ε_2 which can not compare with some typical semiconductors such as Si and GaAs. From equation (4), we can obtain that when $\omega = 0$, ε_2 has a definite effect on the static dielectric constant. Generally ε_1 is obtained by the integration of ε_2 over ω and should naturally relate to the whole shape of ε_2. However for simplicity, here we only discuss the relation between interband transition and the peak of ε_2.

For comparison, γ-Si_3N_4, γ-Ge_3N_4 and γ-$GeSi_2N_4$, which have the same component elements, are also selected to discuss. The relation among energy gap, peak of ε_2 and percentage of Si in formula is presented in Figure 6. The squares stand for the peaks of ε_2 and circles for energy gap. One can see that trend of the peak of ε_2 is contrary to the one of energy gap with respect to Si percentage. Nevertheless, though the band gap increases much from γ-$SiGe_2N_4$ to γ-$GeSi_2N_4$, the ε_2 peak does not decrease as much as band gap correspondingly. It can be obtained that the band gap plays a more important role in ε_2 peak while the matrix element effect is less [41].

The peak value of ε_2 is located at a photon energy to which many band transitions correspond. The band transitions with the largest contribution to the peak of ε_2 are shown as black arrows in Figures 2a and 2b. The transition bands are provided in Table 5. According to our analysis, the initial band is mostly composed of N-2p. Whereas excluding the contribution of N atoms, the ending band is dominated by octahedrally coordinated cations except for γ-Si_3N_4, in which tetrahedrally coordinated Si takes a more important part. In γ-$SiGe_2N_4$ the ending band is mostly occupied by Ge-4p and Si-p states decreasingly regardless of the effect of N-p states.

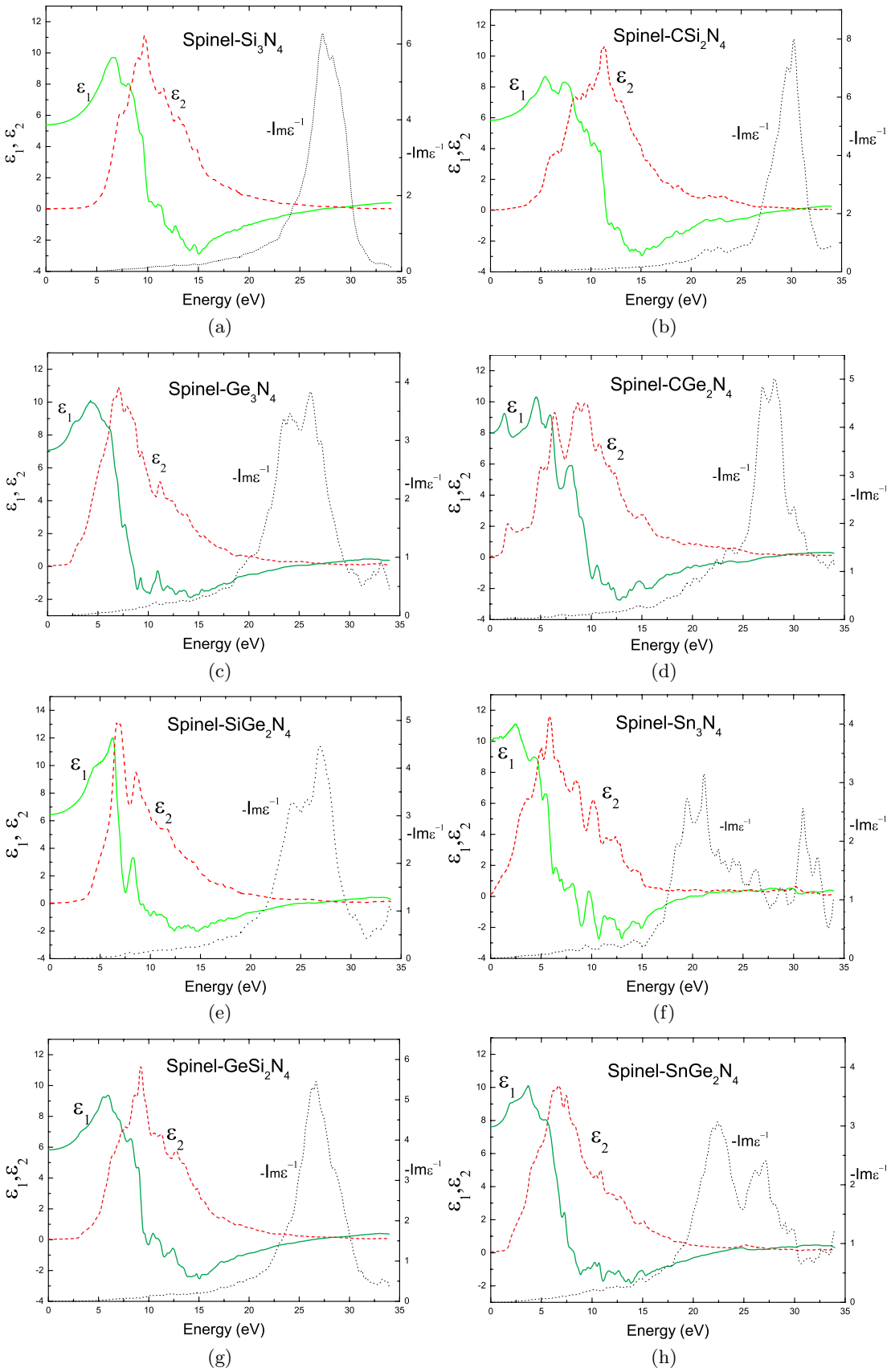

Fig. 5. Dielectric function $\varepsilon_1(\omega)$, $\varepsilon_2(\omega)$ and energy loss function of (a) γ-Si_3N_4, (b) γ-CSi_2N_4, (c) γ-Ge_3N_4, (d) γ-CGe_2N_4, (e)γ-$SiGe_2N_4$, (f) γ-Sn_3N_4, (g) γ-$GeSi_2N_4$, (h) γ-$SnGe_2N_4$.

Table 5. Band transition of maximum contribution to ε_2 peak.

Crystal	Band transition(main component)		Critical **k**-point
	initial	ending	
γ-Si_3N_4	30(N)	40(Si_{tet})	(0.39396, 0, 0)
γ-Ge_3N_4	57(N)	68(N,Ge_{oct})	(0.28989, 0.19993, 0.10996)
γ-$SiGe_2N_4$	58(N)	66(N,Ge)	(0.10209, 0, 0)
γ-$GeSi_2N_4$	54(N)	64(N,Si)	(0.4177, 0.08354, 0)
γ-CSi_2N_4	36(N,C)	53(N,Si)	(0.24698, 0, 0)
γ-CGe_2N_4	52(N,Ge)	65(N,Ge)	(0.27786, 0.21374, 0.14962)
γ-Sn_3N_4	80(N)	88(N,Sn)	(0.32706, 0.21804, 0)
γ-$SnGe_2N_4$	65(N,Ge)	75(N,Ge)	(0.11613, 0.11613, 0.11613)

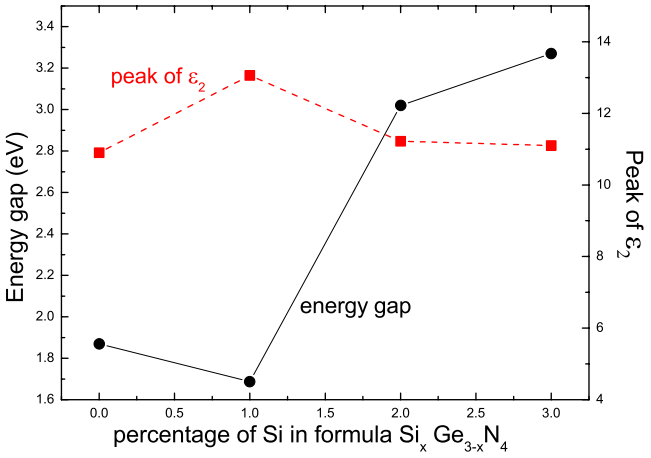

Fig. 6. (Color online) Relation among peak of ε_2, band gap and percentage of Si in formula $Si_xGe_{3-x}N_4$. The black solid circle is for band gap and red square for peak of ε_2. 0, 1.0, 2.0 and 3.0 in x-axis are for γ-Ge_3N_4, γ-$SiGe_2N_4$, γ-$GeSi_2N_4$ and γ-Si_3N_4 respectively.

This fact leads to an assumption that changing the number of p-electrons of cations at Ge(oct)-site or Si(tet)-site could induce the re-distribution of the energy band, especially the bottom of the conduction band or top of the valence band, which in turn varies the energy difference and the number of states of the interband transitions, then results in an alteration in the peak of ε_2. So it is encouraged that the substitution of appropriate atoms can take an effect on the ε_2 peak.

4 Conclusions

According to our calculations by FLAPW, we concluded that in double spinel nitrides, γ-CSi_2N_4, γ-$GeSi_2N_4$ and γ-$SiGe_2N_4$ are stable. γ-Sn_3N_4 has a narrow band gap and a normal bulk modulus. In double spinel nitrides, it is apparent that the element in octahedrally coordinated sites takes a more important part in the band gap. The band gap narrows as valence electron number in octahedrally coordinated cations increases.

Our calculations show that γ-$SiGe_2N_4$ can be a semiconductor with extremely interesting properties with potential technological applications. It has a large bulk modulus of 241.7 GPa and a very favorable direct band gap of 1.58 eV. It also has a large static dielectric constant and high peak value of ε_2. The band transitions which have the largest contribution to the peak of ε_2 have been identified for eight materials. The component of initial and ending bands are analyzed. An assumption is proposed to raise the peak of ε_2.

References

1. V.I. Belyi, *Material Science Monographs* (Elsevier, New York, 1988), Vol. 34
2. R.N. Katz, Science **208**, 841 (1980)
3. I. Kohastu, J.W. McCauley, Mater. Res. Bull. **9**, 917 (1974)
4. H.F. Priest, F.C. Burns, G.L. Priest, E.C. Skaar, J. Am. Ceram. Soc. **56**, 395 (1973)
5. O. Borgen, H.M. Seip, Acta Chem. Scand. **15**, 1789 (1961)
6. S. Wild, P. Grieveson, K.H. Jack, Spec. Ceram. **5**, 385 (1972)
7. A. Zerr, G. Miehe, G. Serghiou, M. Schwartz, E. Kroke, R. Riedel, H. Fuess, P. Kroll, R. Boehler, Nature **400**, 340 (1999)
8. H. Wang, Y. Chen, Y. Kaneta, S. Iwata, J. Phys.: Condens. Matter **18**, 10663 (2006)
9. G. Serghiou, G. Miehe, A. Tschauner, A. Zerr, R. Boehler, J. Chem. Phys. **111**, 4659 (1999)
10. T. Sekine, H. He, T. Kobayashi, M. Zhang, F. Xu, Appl. Phys. Lett. **76**, 3706 (2000)
11. J. Dong, O.F. Sankey, S.K. Deb, G. Wolf, P.F. McMillan, Phys. Rev. B **61**, 11979 (2000)
12. D.M. Teter, R.J. Hemley, Science **271**, 53 (1996)
13. M. Shemkunas, G.H. Wolf, K. Leinenweber, W.T. Petuskey, J. Am. Ceram. Soc. **85**, 101 (2002)
14. N. Scotti, W. Kockelmann, J. Senker, S. Trassel, H. Jacobs, Z. Anorg. Allg. Chem. **625**, 1435 (1999)
15. L. Maya, Inorg. Chem. **31**, 1958 (1992)
16. P.R. Coffman, *Synthesis, processing and characterization of several group IV, V and VI nitrides and related compounds*, Ph.D. Dissertation, Arizona State University, 1996, pp. 89–107
17. L. Maya, J. Vac. Sci. Technol. A **11**, 604 (1993)
18. T. Maruyama, T. Morishita, J. Appl. Phys. **77**, 6641 (1995)

19. T. Maruyama, T. Morishita, Appl. Phys. Lett. **69**, 890 (1996)
20. Y. Inoue, M. Nomiya, O. Takai, Vacuum **51**, 673 (1998)
21. N. Takahashi, K. Terada, T. Nakamura, J. Mater. Chem. **10**, 2835 (2000)
22. S.D. Mo, L. Ouyang, W. Ching, I. Tanaka, Y. Koyama, R. Riedel, Phys. Rev. Lett. **83**, 5046 (1999)
23. W.Y. Ching, S.D. Mo, L. Quyang, Phys. Rev. B **63**, 245110 (2001)
24. W.Y. Ching, S.D. Mo, L. Ouyang, I. Tanaka, M. Yoshiya, Phys. Rev. B **61**, 10609 (2000)
25. W.Y. Ching, S.D. Mo, L. Quyang, P. Rulis, J. Am. Ceram. Soc. **85**, 75 (2002)
26. J.P. Perdew, Y. Wang, Phys. Rev. B **45**, 13244 (1992)
27. J.P. Perdew, K. Burke, M. Ernzerhof, Phys. Rev. Lett. **77**, 3865 (1996)
28. P. Blaha, K. Schwarz, G.K.H. Madsen, D. Kvasnicka, J. Luitz, ***WIEN2k*** *An Augmented Plane Wave + Local Orbitals Program for Calculating Crystal Properties* (Karlheinz Schwarz, Techn. Universität Wien, Austria, ISBN 3-9501031-1-2, 2001)
29. K. Schwarz, P. Blaha, G.K.H. Madsen, Computer Phys. Commun. **147**, 71 (2002)
30. P.E. Blochl, O. Jepsen, O.K. Andersen, Phys. Rev. B **49**, 16223 (1994)
31. P.A. Fox, A.D. Hall, N.L. Schryer, ACM Trans. Math. Software, New York, 1978, Vol. 4
32. H.J. Grenville-Wells, K. Lonsdale, Nature **181**, 758 (1958)
33. G.K.H. Madsen, P. Blaha, K. Schwarz, E. Sjöstedt, L. Nordström, Phys. Rev. B **64**, 195134 (2001)
34. W.Y. Ching, P. Rulis, Phys. Rev. B **73**, 045202 (2006)
35. M. Shemkunas, W.T. Petuskey, A.V.G. Chizmeshya, K. Leinenweber, G.H. Wolf, J. Mater. Res. **19**, 1392 (2004)
36. J. Dong, J. Deslippe, O.F. Sankey, E. Soignard, P.F. McMillan, Phys. Rev. B **67**, 094104 (2003)
37. J.F. Jansen, A.J. Freeman, Phys. Rev. B **30**, 561 (1984)
38. L. Hedin, Phys. Rev. **139**, A796 (1965)
39. H.A. Kramers, Nature **117**, 775 (1926)
40. R.d.L. Kronig, J. Opt. Soc. Am. **12**, 547 (1926)
41. N. Christensen, B. Seraphin, Phys. Rev. B **4**, 3321 (1971)